Multitarget thiol-activated tetrapyridyl gold(III) complexes for hypoxic cancer therapy

Zhou, X.; Abyar, S.; Carbo-Bague, I.; Wang, L.; Türck, S.; Siegler, M.A.; ... ; Bonnet, S.A.

CCS Chemistry

RESEARCH ARTICLE

Received: July 13, 2023 | Accepted: Oct. 23, 2023 | Published: Dec. 1, 2023

Multitarget Thiol-Activated Tetrapyridyl Gold(III) Complexes for Hypoxic Cancer Therapy

Xue-Quan Zhou[1,2]*, Selda Abyar[2], Imma Carbo-Bague[2,3], Lan Wang[2], Sebastian Türck[4], Maxime A. Siegler[5], Uttara Basu[4], Ingo Ott[4], Rongfang Liu[6], Adriaan P. IJzerman[6] & Sylvestre Bonnet[2]*

[1]*Institute of Biopharmaceutical and Health Engineering, Tsinghua Shenzhen International Graduate School (SIGS), Tsinghua University, Shenzhen 518055,* [2]*Leiden Institute of Chemistry, Leiden University, 2333 CC Leiden,* [3]*Department of Chemistry, Simon Fraser University, Burnaby, British Columbia V5A 1S6,* [4]*Institute of Medicinal and Pharmaceutical Chemistry, Technische Universität Braunschweig, 38106 Braunschweig,* [5]*Department of Chemistry, Johns Hopkins University, Baltimore, Maryland 21218,* [6]*Division of Drug Discovery & Safety, Leiden Academic Centre for Drug Research, Leiden University, 2333 CC Leiden*

**Corresponding authors: xuequan_zhou@163.com; bonnet@chem.leidenuniv.nl*

Cite this: *CCS Chem.* **2024**, 6, 783–797
DOI: 10.31635/ccschem.023.202303190

Gold complexes have emerged as promising anticancer metallodrugs due to their efficient thioredoxin reductase (TrxR) inhibition, which disturbs the redox balance of cancer cells. However, in this model, the role of the ligand(s) coordinated to gold is often overlooked. In this work, we present a series of tetrapyridyl Au(III) complexes that exhibit thiol-induced release of a Au(I) ion and a tetrapyridyl ligand. The formation of a free Au(I) center is responsible for the expected TrxR inhibition. Additionally, the released ligand, which was visible in cells due to its intense blue fluorescence, showed excellent binding properties to the hERG potassium channel. Moreover, these ligands ended up in the lysosomes, resulting in significant lysosome damage. Altogether, the Au(III) complexes presented in this work showed broad-spectrum anticancer properties, both in hypoxic 2D monolayers and 3D tumor spheroids. We suggest that the interaction of the released Au(I) center and the tetrapyridyl ligand with two different protein targets may combine into prodrugs that overcome hypoxia-induced drug deactivation.

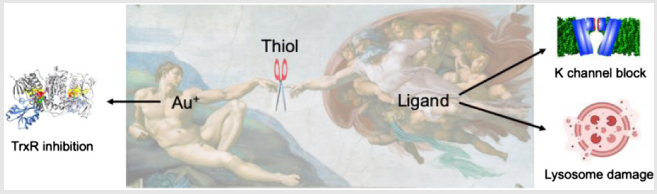

Keywords: **anticancer Au(III) complexes, enzyme inhibtion, potassium channel affinity, lysosome damage, cell imaging, prodrug**

Introduction

The success of cisplatin in the treatment of cancer has stimulated the development of anticancer metallodrugs for decades, aiming at improved efficiency, lower side effects, and reduced drug resistance.[1–9] Gold complexes, in particular, have shown potent anticancer activities that often overcome cisplatin limitations due to their different mode of action (MOA).[10–17] One of the exquisite MOAs for gold anticancer complexes is that they target biomolecules containing selenothiol and thiol moieties, especially thioredoxin reductase (TrxR) and glutathione (GSH).[10,18,19] This selectivity arises from the robust interaction between gold ions and the chalcogenide atoms of these biomolecules.[20] Since TrxR is overexpressed in many types of cancer cells,[19,21–24] and the TrxR/GSH system is one of the major cellular defense lines against oxidative stress resulting from high reactive oxygen species levels, this system is known as a good molecular target for anticancer therapy.[22,23,25,26] Auranofin, a Au(I)

compound characterized by a phosphine and a thiolate ligand in a linear geometry, is approved for the treatment of rheumatoid arthritis. It has more recently been thoroughly investigated as an anticancer drug, for which its affinity and inhibition properties towards TrxR are an asset.[27] This drug is known to release, after losing its organic ligands, electrophilic gold(I) ions, which react selectively with the selenocysteine residues in the active site of the TrxR enzyme, to end up trapped into the binding site, thereby blocking its function.[26–28] A molecular docking study demonstrated that the Au(I) ion may form a stable, irreversibly coordinated Cys–Au(I)–Cys complex that permanently inhibits the catalytic function of TrxR enzyme in many human pathogens.[29] Based on these ideas, many Au(I) complexes have been developed over the years,[30,31] especially those based on *N*-heterocyclic carbene ligands.[32–39]

Extensive research efforts have highlighted the fact that Au(III) complexes also have the capability to release Au(I) ions intracellularly, primarily because they undergo reduction by intracellular thiols after cellular uptake.[40] The reduction process is often accompanied by the release of the initially coordinated ligands.[18,40] Although the inhibiting properties of the Au(I) ions released against TrxR or other thiol-containing proteins have been well documented, the scarcity of the research dedicated to exploring the biological activities of these released organic ligands is noticeable. In principle, some synergistic effects can be expected if the ligands released by the reduction of a Au(III) prodrug are selective inhibitors of specific proteins overexpressed in cancer cells. Polypyridyl ligands have been widely used to coordinate metal complexes, as they offer various denticities and can easily be functionalized with different functional groups.[19,41] Further, they belong to the larger family of *N*-heterocyclic ligands, which are found in roughly 60% of U.S. Food and Drug Administration-approved drugs.[42] In fact, many *N*-heterocyclic ligands have been investigated for their ability to regulate potassium channels.[43–45] Potassium channels are transmembrane proteins that selectively facilitate the flow of potassium ions down its electrochemical gradient. They have gained recognition as an emerging target in cancer therapy for their specific functions in cell proliferation, the control they exert on cell cycle progression, and their overexpression in several forms of cancer.[46,47]

Therefore, we envisioned that the combination of TrxR inhibitors and potassium channel inhibitors in a single molecule may be proposed as a new strategy for chemotherapy. Furthermore, we realized that the fluorescence of many polypyridyl ligands, which is often quenched by metal complexation, can be recovered after ligand release. This restoration would enable visualization of the organelle targeted by such compounds. Herein, we investigated the relevance of this analysis by preparing three tetrapyridyl Au(III) complexes based on *N*,*N*-bis(2-2′-bipyrid-6-yl)amine (**Hbbpya**), *N*6,*N*6′-di(pyridin-2-yl)-2,2′-bipyridine-6,6′-diamine (**H_2bapbpy**), and 6,6-bis[*N*-(isoquinolyl)-1-amino]-2,2-bipyridine (**H_2biqbpy**), and by evaluating their intracellular localization, their thiol-dependent reduction and ligand release properties, their cytotoxicity, and their TrxR/human ether-à-go-go related gene (hERG) inhibition properties.

Experimental Methods

General information

All syntheses were performed in a dinitrogen atmosphere as described in the Supporting Information. All the chemical compounds and the other materials were purchased from Sigma-Aldrich (Amsterdam, The Netherlands). All reactants and solvents were used without further purification. All ^{1}H NMR and ^{13}C attached-proton-test NMR spectra were recorded on a Bruker DPX-300 or DMX-400 spectrometer Chemical shifts were indicated in ppm relative to the residual solvent peak. Electrospray ionization mass spectra (ESI-MS) were recorded by using an MSQ Plus Spectrometer positive ionization mode. High-resolution mass spectra of two palladium complexes were recorded on a Waters XEVO-G2 XSQ-TOF mass spectrometer equipped with an electrospray ion source in positive mode (source voltage 3.0 kV, desolvation gas flow 900 L/h, temperature 250 °C) with resolution R = 22,000 (mass range m/z = 50–2000) and 200 pg/μL Leu-enkephalin (m/z = 556.2771) as a "lock mass." UV–vis spectra were recorded on a Cary 50 spectrometer from Varian (Amsterdam, The Netherlands). Human cancer cell lines A549 (human lung carcinoma), A431 (human skin carcinoma), A375 (human melanoma), and MCF-7 (human breast carcinoma) were purchased from Sigma-Aldrich, distributed by the European Collection of Cell Cultures. Dulbecco's modified Eagle medium (DMEM, with and without phenol red, without glutamine), Glutamine-S (GM; 200 mm), tris(hydroxylmethyl)aminomethane (Tris base), trichloroacetic acid, glacial acetic acid, and sulforhodamine B (SRB) were also purchased from Sigma-Aldrich. The measurements of complexes on cytotoxicity were performed according to the literature.[48] More details of the experiments are described in Supporting Information.

Single-crystal X-ray crystallography

Excess KPF_6 was added into a MilliQ water solution of **[2]Cl** and **[3]OAc** to make a precipitate of **[2]PF_6** and **[3]PF_6**, which were used for single crystal preparation. The single crystals of **[1]Cl_2**, **[2]PF_6**, and **[3]PF_6** were obtained by slow evaporation of ether into a saturated dichloromethane (DCM)/MeOH (1:1) solution of **[1]Cl**, **[2]PF_6**, and **[3]PF_6**. All reflection intensities were measured at 110(2) K using a SuperNova diffractometer (Yarnton, Oxfordshire, UK; equipped with an Atlas detector)

DOI: 10.31635/ccschem.023.202303190
Citation: *CCS Chem.* **2024**, 6, 783–797
Link to VoR: https://doi.org/10.31635/ccschem.023.202303190

with Mo *K*α radiation (λ = 0.71073 Å) under the program CrysAlisPro (Version CrysAlisPro 1.171.39.29c, Rigaku OD, 2017). The same program was used to refine the cell dimensions and for data reduction. The structures were solved with the program SHELXS-2014/7[49] and was refined on F^2 with SHELXL-2014/7.[49] Numerical absorption correction based on Gaussian integration over a multi-faceted crystal model was applied using CrysAlisPro (Yarnton, Oxfordshire, UK). The temperature of the data collection was controlled using the system Cryojet (manufactured by Oxford Instruments, Yarnton, Oxfordshire, UK). The H atoms were placed at calculated positions (unless otherwise specified) using the instructions AFIX 43 with isotropic displacement parameters having values 1.2 *U*eq of the attached C atoms. The Cambridge Crystallographic Data Centre numbers for **[1]Cl$_2$**, **[2]PF$_6$**, and [**3]PF$_6$** are 2221581, 2221580, and 2221582, respectively.

[1]Cl$_2$: The structure is ordered. There are two lattice water solvent molecules in the asymmetric unit, and the H atoms were found from difference Fourier maps. Their coordinates were refined pseudofreely using the DFIX instructions in order to keep the O–H and H . . . H distances within some acceptable ranges. The difference Fourier map shows no residual electron density peak near N3, which indicates that N3 is not protonated. Furthermore, the C–N–C distances (1.343(3) and 1.337(3) Å) were significantly shorter than those found for typical C–NH–C.

[2]PF$_6$: The structure is ordered. The crystal that was mounted on the diffractometer was nonmerohedrally twinned, and the twin relationship corresponds to a twofold rotation around the **c*** reciprocal direction. The BASF scale factor refines to 0.5352(10).

[3]PF$_6$: The structure is ordered. The crystal that was mounted on the diffractometer was pseudo-merohedrally twinned (the monoclinic unit cell mimics an orthorhombic cell). The twin relationship corresponds to a twofold axis along the *c* direction, and the BASF scale factor refines to 0.4171(18).

pK_a determination

Method

A range of buffer solutions of different pH values (0.3–11) were prepared according to the literature.[1] Minor modifications were introduced in the method to include buffer solutions at lower pHs. We used an HCl solution for the pH range 0.3–1, an HCl/KCl solution for pH 1–2, a citric acid/citrate for pH 2.2–3.4, an acetic acid/sodium acetate for pH 3.5–5.5, and a KH_2PO_4/K_2HPO_4 for pH 6–9, and smaller pH intervals of 0.2–0.3 units in the range pH 1.0–7.0 compared to the literature procedure. The ionic strength of all buffered solutions, except for the range pH 0.3–1, was adjusted to *I* = 0.1 M with a KCl solution, and the pH was experimentally measured with a pH-meter for all solutions with pH > 1.0. Then 196 μL of each buffer solution was added to each well in a 96-well plate, building a sequence of increasing pH values over each line A, B, C, D, and so on in the plate (Supporting Information Scheme S1). Then, 4 μL of a stock solution (1 Mm, Milli-Q water) of each complex [1]Cl_2, [2]Cl, or [3]OAc was added to each well to reach a complex concentration of 20 μM. After 5 min, the absorbance (300–600 nm) of all 96 solutions of the plate at different pH values was recorded using a M1000 TeCan Reader.

Analysis

The absorbance of each complex depends on the concentration of the different protonated forms of the complexes. The equation $Abs_{\lambda1}/Abs_{\lambda2} = ([H^+] + c_1 \times K_a)/(c_2 \times [H^+] + c_3 \times K_a)$ was used to remove the operating error on the concentrations, in which λ_1 = 419, 371, and 402 nm, and λ_2 = 360, 333, and 359 nm for **[1]Cl$_2$**, **[2]Cl** and **[3]OAc**, respectively, and c_1, c_2, c_3 are the concentration of H_2A, HA^-, and A^{2-}. Then the *X*–*Y* scatter diagrams of pH-$Abs_{\lambda1}/Abs_{\lambda2}$ data were fitted by the [Inhibitor] versus response-variable slope (four parameters) nonlinear fitting equation: Y = bottom + (top – bottom)/(1 + $(IC_{50}/X)^{HillSlope}$). The IC_{50} values calculated by this fitting procedure were considered as pK_a values.

Gold cellular uptake by inductively coupled plasma-mass spectrometry

A549 cells were seeded in a 12-well plate (2×10^5 cells, 1 mL Opti-MEM complete per well). At *t* = 24 h, the cells were treated with complexes **[1]Cl$_2$**, **[2]Cl**, or **[3]OAc** (1 μM, 0.5 mL Opti-MEM complete). After 24 h treatment, the cells were washed once with phosphate-buffered saline (PBS) and harvested by trypsin (5% v/v in PBS), counted via trypan blue on a TC20™ automated cell counter, and centrifuged in 15 mL tubes. After removing the supernatant, the cell pellets were lysed by adding 0.5 mL HNO_3 (65%) into the tubes, keeping them for 10 min and sonicating them for 30 min at room temperature. After that, the cell solution was diluted to 10 mL using Milli-Q water, and the Au content in the solution was determined by inductively coupled plasma-mass spectrometry (ICP-MS; NexION 2000, PerkinElmer, Drachten, The Netherlands). The final results are the mean of three independent experiments. The errors have been calculated by the standard error of the mean.

ICP-MS measurement protocol

Materials

Nitric acid (65%, Suprapur®, Merck, Amsterdam, The Netherlands) was used in the sample digestion process, while diluted (3.25%) nitric acid was used as a carrying solution throughout the ICP measurements. National Institute of Standards and Technology (NIST)-traceable 1000 mg/L elemental standards were used (TraceCERT®, Fluka, Amsterdam, The Netherlands) for preparation of

DOI: 10.31635/ccschem.023.202303190
Citation: *CCS Chem.* **2024**, 6, 783–797
Link to VoR: https://doi.org/10.31635/ccschem.023.202303190

calibration and internal standards. Approximately 18 MΩ cm^{-1} water (MiliQ) was used in all sample preparation and analysis steps.

Instrumentation

Calibration standards were prepared in a Secuflow fumehood (SCALA, Waldner, Duizel, The Netherlands) to prevent contamination by atmospheric particulates. The standard samples and measurement samples were analysed for trace elements using the NexION® 2000 (PerkinElmer) ICP-MS equipped with a concentric glass nebulizer and Peltier-cooled glass spray chamber. An SC2 DX autosampler (PerkinElmer) was connected to the ICP-MS for sample introduction. Syngistix™ software for ICP-MS (v.2.5, PerkinElmer) was used for all data recording and processing.

Elemental analysis

Five trace elemental calibration standards for ICP-MS analysis were prepared using NIST-traceable 1000 mg/L Au standards: 0, 1, 4, 20, 100 μg/L. To check the calibration, samples were analyzed consisting of a blank measurement and a repeat measurement of one of the calibration standards. For the calibration curve only to be accepted as correlation coefficient (Cor.Coeff), it was found higher than 0.999.

Flow cytometry

2×10^5 A549 cells (1 mL Opti-MEM complete) were first seeded on 12-well plates and incubated for 24 h in normoxic conditions (21% O_2, 7% CO_2, and 100% H_2O). For apoptosis experiments, the cells were then treated with cisplatin (15 μM) or gold complexes (10 μM) for 24 h. Then the cells were harvested and double-stained by annexin V (5 μL, Abcam, Amsterdam, The Netherlands) and propidium iodide (PI, 5 μL, Abcam) for 15 min. The cell emission signals were detected by flow cytometry according to the commercial product protocol (Abcam). For lysosome damage determination, the cells were treated with *t*-BuOOH (0.6 mM) and the gold complexes (at 5xEC_{50}) for 4 h. Then the cells were harvested and double-stained by LysoTracker™ Green (LTG) DND-26 ((*N*-[2-(dimethylamino)ethyl]-3-{2-[(3,5-dimethyl-1H-pyrrol-2-yl-κN)methylidene]-2H-pyrrol-5-yl-κN}propanamidato)(difluoro)boron; 100 nM, 30 min) and PI (5 μL, 15 min). The cell emission signals were measured by flow cytometry using the green-blue channel for LTG and red-blue channel for PI. The data were analyzed by FlowJo 10.

Confocal experiments

200 μL aliquots containing 2×10^4 A549 cells were first seeded onto a μ-slide 8-well confocal plate (ibidi). At t = 24 h, each well was treated with **[1]Cl_2**, **[2]Cl**, or **[3]OAc** (20 μM, Opti-MEM complete). At t = 27 h, wells were treated with LTG DND-26 (100 nM, in Opti-MEM complete) for 30 min. Then the cells were washed with PBS once, and the emission of the cells was imaged at two excitation channels (ex 405 nm/em 410–460 nm and ex 488 nm/em 500–460 nm) using a Leica SP8 confocal microscope (Amsterdam, The Netherlands). Images were analyzed using ImageJ.

TrxR inhibition in aqueous solution

To determine the inhibition of mammalian TrxR, a spectrophotometric assay was done using commercially available rat liver TrxR (Sigma-Aldrich). The enzyme was diluted with distilled water to achieve a concentration of 2.5 U/mL. The gold complexes were freshly dissolved dimethylformamide (DMF) to get a stock solution of 10 mM. To a 25 μL aliquot of the enzyme solution, 25 μL of potassium phosphate buffer, pH 7.0, containing the complexes at different concentrations or vehicles (DMF) without compounds (control probe) was added, and the resulting solutions (final concentration of DMF: max. 0.5% v/v) were incubated with moderate shaking for 75 min at 37 °C in a 96-well plate. Subsequently, to each well, 225 μL of the reaction mixture (1000 μL of reaction mixture consisted of 500 μL of potassium phosphate buffer, pH 7.0, 80 μL of ethylenediaminetetraacetic acid (EDTA) solution (100 mM, pH 7.5), 20 μL of bovine serum albumin (BSA) solution (0.2%), 100 μL of nicotinamide adenine dinucleotide phosphate (NADPH) solution (20 mM), and 300 μL of distilled water) was added. The reaction was started by the addition of 25 μL of an ethanolic 5,5′-dithiobis 2-nitrobenzoic solution (DTNB, 20 mM). After proper mixing, the formation of 5-TNB was monitored with a microplate reader (Perkin-Elmer Victor X4; Perkin Elmer, Waltham, Massachusetts, USA) at 405 nm in 10 s intervals for 10 min. The increase in 5-TNB concentration over time followed a linear trend ($R^2 \geq 0.99$), and the enzymatic activities were calculated as the slopes (increase in absorbance per second) thereof. For each tested compound, the noninterference with the assay components was confirmed by a negative control experiment using an enzyme-free solution. The IC_{50} values were calculated as the concentration of complexes decreasing the enzymatic activity of the untreated control by 50% and were given as the means and standard deviations of two independent experiments.

Inhibition of TrxR in cells

The TrxR inhibition assay for the compounds was tested on A549 cells. Briefly, cells were seeded in 24-well plates at a density of 1×10^5 cells/well in DMEM/10% fetal bovine serum. After 24 h, they were treated with varied concentrations of the compounds dissolved in DMF (0.1%) and incubated at 37 °C, 5% CO_2 for 24 h. Following this, the media were removed, cells were washed twice with cold

DOI: 10.31635/ccschem.023.202303190
Citation: *CCS Chem.* **2024**, 6, 783–797
Link to VoR: https://doi.org/10.31635/ccschem.023.202303190

PBS, and lysed with ice-cold lysis buffer (50 mM phosphate buffer pH 7.4; 1 mM EDTA, 0.1% Triton-X 100) for 30 min on ice. The protein content in the samples was estimated using Bradford assay with BSA as the calibration standard. Equal amounts of protein (10 μg) were used. Samples were incubated with 30 μL reaction mixture (HEPES buffer (0.2 mM), insulin (3 mg/mL), NADPH (1 mM), EDTA (2 mM), and either 10 μL recombinant thioredoxin (1 mg/mL) or 10 μL 4-(2-hydroxyethyl)-1-piperazineethanesulfonic acid (HEPES) buffer (200 μM) for 20 min at 37 °C). The reaction was stopped with 200 μL stopping solution containing guanidine hydrochloride (5.4 M in Tris–HCl 100 mM) and 5,5′-dithiobis(2-nitrobenzoic acid) (1 mM). The absorbance was measured at 405 nm using a PerkinElmer VICTOR X4 (Perkin Elmer, Waltham, Massachusetts, USA) plate reader. The difference in the absorbance of samples containing Trx and buffer gives the activity due to TrxR. The data were analyzed, and IC_{50} values were determined using nonlinear curve fit with Origin 8.0 (OriginLab Corporation, Northampton, Massachusetts, USA).

K_v11.1 potassium channel binding affinity

This experiment was carried out according to a literature procedure.[50] Briefly, cell membranes of HEK293 K_v11.1 cells were collected. Membrane aliquots containing 30 μg protein were incubated with 4 nM [^{3}H]dofetilide in a total volume of 100 μL incubation buffer (10 mM HEPES, 130 mM NaCl, 60 mM KCl, 0.8 mM $MgCl_2$, 1 mM EGTA, 10 mM glucose, 0.1% BSA, pH 7.4) at 25 °C for 60 min. At this concentration, total radioligand binding did not exceed 10% of the radioligand added to prevent ligand depletion. Nonspecific binding was determined in the presence of 10 μM astemizole. [^{3}H]Dofetilide did not bind to membranes prepared from empty HEK293 cells lacking the K_v11.1 channel (data not shown). All compounds were tested at one concentration of 10 μM. Incubations were terminated by dilution with ice-cold wash buffer (25 mM Tris, 130 mM NaCl, 60 mM KCl, 0.8 mM MgCl2, 0.05 mM $CaCl_2$, 0.05% BSA, pH 7.4). Separation of bound from free radioligand was performed by rapid filtration through a 96-well GF/B filter plate using a PerkinElmer Filtermate-harvester (PerkinElmer, Groningen, the Netherlands). Filters were subsequently washed 12 times with ice-cold wash buffer. The filter-bound radioactivity was determined by scintillation spectrometry using the P-E 2450 Microbeta2 counter (PerkinElmer) after addition of 25 μL Microscint and 3 h extraction.

Results and Discussion

Synthesis and crystal structure

The ligands Hbbpya, H_2bapbpy, and H_2biqbpy were synthesized according to the literature.[51,52] They were then coordinated to Au(III) by refluxing a MeOH solution of $NaAuCl_4$ and the ligand in a 1:1 molar ratio. The resulting black suspension was filtered and purified via column chromatography or washing with ethyl acetate, to obtain NMR-pure samples. It is worth noting that following this simple procedure the nature of the counterion was not very well defined, as we found $AuCl_4^-$, $AuCl_2^-$, or Cl^- depending on the tetrapyridyl ligand used.[53] Thus, a chloride ion exchange column was used in the end of the synthesis, to isolate the chloride salts, that is, [Au(bbpya)]Cl_2 ([**1**]**Cl_2**), [Au(bapbpy)]Cl ([**2**]**Cl**), and [Au(biqbpy)]Cl ([**3**]**Cl**). Though **[1]Cl_2** and **[2]Cl** were both water-soluble, **[3]Cl** was not, which is a problem for biological applications. We hence realized an acetate ion exchange by reacting **[3]Cl** with AgOAc, to afford the partially water-soluble salt **[3]OAc**. In this report, the three gold complexes **[1]Cl_2**, **[2]Cl**, and **[3]OAc** were fully charactizated by NMR, mass spectrometry, elemental analysis, and infrared spectra (Supporting Information Figures S1–S4) and used for further biochemical evaluation (Figure 1a). The detailed syntheses and characterization are described in the Supporting Information.

Single crystals of **[1]$^{2+}$** were obtained with various counterions, that is, $AuCl_4^-$, $AuCl_2^-$, and Cl^-, while the crystals of **[2]$^+$** and **[3]$^+$** were obtained with PF_6^- counterions. The crystallographic information and selected bonds and angles for **[1]Cl_2**, **[2]PF_6**, and **[3]PF_6** are described in Supporting Information Tables S1–S4. **[1]Cl_2** and **[2]PF_6** were crystallized in the triclinic *P-1* space group, while **[3]PF_6** was crystallized in the monoclinic $P2_1/n$ space group. In all crystal structures, the noncoordinated amine bridges of the ligands were found deprotonated (Figure 1b), as demonstrated by the bicationic charge of **[1]$^{2+}$** and the monocationic charge of **[2]$^+$** and **[3]$^+$**. This deprotonation is interpreted as a consequence of the high electrophilicity of the Au(III) center, which draws the electron density of the conjugated ligand, thereby making the NH bridges very acidic.[54] The Au–N bond lengths of all complexes were similar, within the range of 1.977–2.044 Å (Supporting Information Table S4). However, **[2]$^+$** and **[3]$^+$** showed much more distorted coordination spheres than **[1]$^{2+}$**, with a higher tetrahedral distortion index τ = 0.179 and 0.167, respectively, compared with τ = 0.109 for **[1]$^{2+}$**. The difference in steric hindrance can be attributed to the presence of two five-membered rings and one six-membered ring in Hbbpya, while H_2bapbpy and H_2biqbpy generate upon coordination only one five-membered ring and two larger six-membered rings.[51] Additionally, the crystal packing (Supporting Information Figure S5) revealed that the gold complexes exhibited significant intermolecular π–π stacking interaction (e.g., intermolecular d(C12…C12′) = 3.361 in [**1**]Cl_2, d(C16-C12′) = 3.223 Å in [**2**]PF_6, and d(C4-C22′) = 3.528 Å in [**3**]PF_6). On the other hand, insertion of the counter anions in the lattice did not allow any Au…Au interaction to occur in the solid state, with intermolecular Au1…Au1′ distances of 8.060 or 8.512 Å in [**1**]Cl_2.2H_2O, 6.555 or 5.366 Å in [**2**]PF_6, and

DOI: 10.31635/ccschem.023.202303190
Citation: *CCS Chem.* **2024**, 6, 783–797
Link to VoR: https://doi.org/10.31635/ccschem.023.202303190

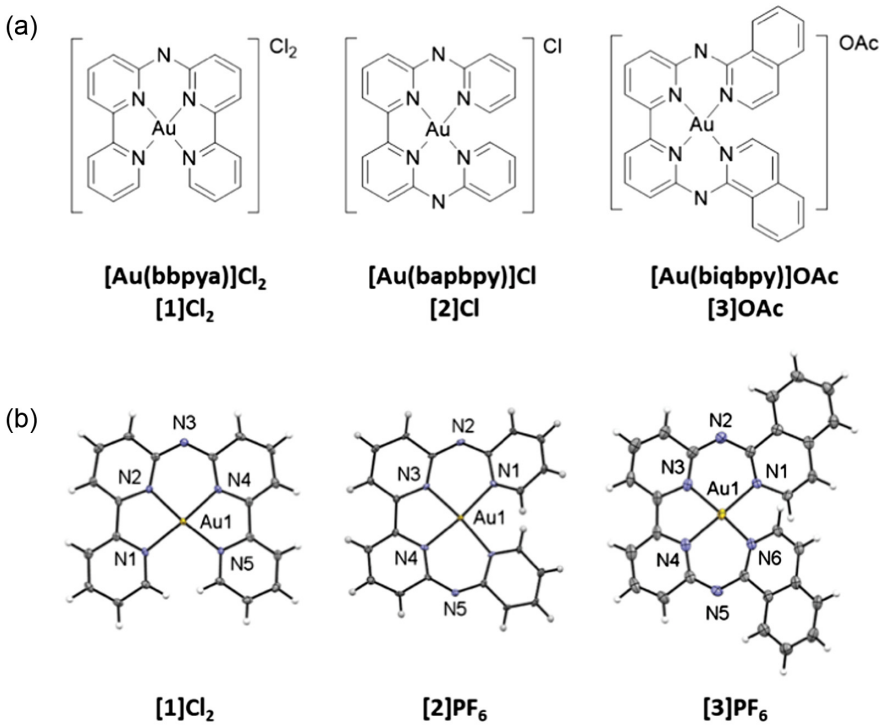

Figure 1 | *(a) Chemical structures of **[1]Cl$_2$**, **[2]Cl**, and **[3]OAc**. (b) Displacement ellipsoid plots (50% probability level) of the cationic parts of the crystal structures of **[1]Cl$_2$**, **[2]PF$_6$**, and **[3]PF$_6$** at 110(2)K. Counter anions and lattice water solvent molecules (only for **[1]Cl$_2$**) are omitted for clarity.*

8.733 or 8.741 Å in [**3**]PF_6. Aurophilic interactions, when present, are known to be weaker with Au(III) centers than with Au(I), Pt(II), or Pd(II) centers,[55] and we did not experience significant supramolecular interaction in aqueous solution with these three complexes, where the gold compounds were essentially soluble.

pK_a determination, thermal stability, and reduction with thiols

The acid–base dissociation constant (pK_a) fuctions as a key physicochemical parameter influencing many biopharmaceutical characteristics of a drug, such as its solubility, cellular uptake, thermal stability, and protein binding strength in a biological environment.[56,57] In the solid state, all three gold complexes were found fully deprotonated, which we interpret as a consequence of the high electrophilicity of the Au(III) center. We determined the pK_a of all three complexes in aqueous solution (20 μM) by UV–vis spectroscopy in buffers at different pH following a published protocol.[58] **[1]Cl$_2$** had a single pK_a value of 2.2, while **[2]Cl** and **[3]OAc** can be deprotonated twice, with a first pK_a1 value of 3.4 and 2.3, respectively, and a second pK_a value of 5.1 and 9.8, respectively (Supporting Information Figure S6 and Table S5). Clearly, the replacement of the terminal pyridyl groups in **[2]$^+$** by quinolyl groups in **[3]$^+$** had a significant influence on the acidity of the amine bridges of these complexes.

All three complexes were stable for 24 h in PBS solution, as demonstrated by their time-independent absorbance spectrum in such conditions (Supporting Information Figure S7). However, after adding GSH in a concentration ratio at 1:2 (50 μM **[1]Cl$_2$**/100 μM GSH), the absorbance of all complexes dramatically changed within 30 s (Supporting Information Figure S8), indicating rapid reaction. The gold complexes showed similar instability upon adding BSA in a concentration ration at 1:4 (50 μM complexes/200 μM BSA, Supporting Information Figure S9). The **[1]Cl$_2$**/GSH system (50 μM/100 μM) in PBS was further monitored for 24 h using absorption spectroscopy as a standard. As shown in Figure 2a, the absorbance band around 425 nm, which belongs to the metal-to-ligand charge transfer (MLCT) of the complex,[59,60] decreased in the first minute of the reaction to completely disappear after 24 h, suggesting the total alteration of the coordination sphere of **[1]Cl$_2$**. Meanwhile, the band at 325 and 270 nm, which belongs to the ligand-to-ligand charge-transfer (LLCT),[59,60] significantly decreased upon 24 h reaction concomitantly with the formation of a precipitate, suggesting the water-insoluble ligand may have been released by the reaction with GSH.

The emission of the **[1]Cl$_2$/GSH** mixture was also compared with that of a solution of the pure complex **[1]Cl$_2$**, **Hbbpya**, or GSH in PBS. As shown in Figure 2b, after 2 min, the emission intensity of **[1]Cl$_2$:GSH** mixture

DOI: 10.31635/ccschem.023.202303190
Citation: *CCS Chem.* **2024**, 6, 783–797
Link to VoR: https://doi.org/10.31635/ccschem.023.202303190

showed a ninefold increase compared with that of **[1]Cl_2** only; the emission peak also matched well with that of the **Hbbpya** ligand, here as well suggesting ligand release in the **[1]Cl_2/GSH** mixture. This thiol-activated fluorescence recovery was also detected for **[2]Cl** and **[3]OAc** (Supporting Information Figure S10), showing that it is a general property of this family of tetrapyridyl Au(III) compounds.

To confirm the hypothesis of ligand release, the reaction of **[1]Cl_2** with GSH was monitored by ^{1}H NMR spectroscopy. As shown in Figure 2c, at t = 2 min, the mixture of [**1**]Cl_2 (3.7 mM) and GSH (7.4 mM) in D_2O showed completely different NMR peaks compared with pure [**1**]Cl_2, suggesting that a reaction had occurred. GSH and glutathione disulfide (GSSG) show very similar ^{1}H NMR spectra with the exception of the proton signals from the cysteine residue.[61] The proton α-H at 4.54 ppm for GSH shifts to 4.72 ppm in GSSG, which usually overlaps with the strong solvent peak of D_2O, and the β_1-H and β_2-H peaks at 2.92 ppm for GSH splits in two dd at 2.94 and 3.24 ppm for GSSG, in agreement with the literature.[61,62] After 24 h, no further change was observed in the ^{1}H NMR

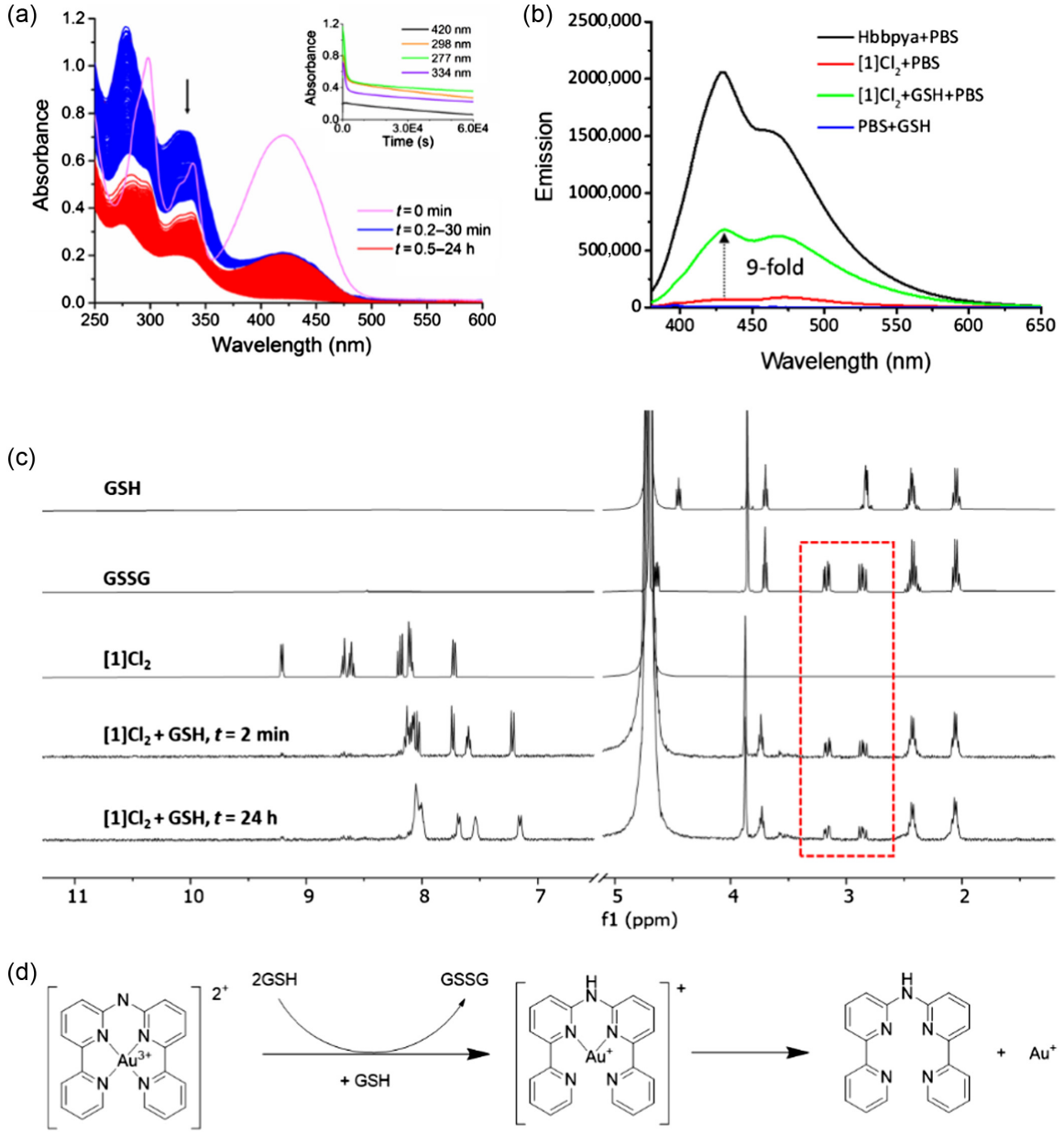

Figure 2 | *(a) Evolution of the absorbance spectra of a mixture of **[1]Cl_2**:GSH (50 μM:100 μM) in PBS solution at 310 K for 24 h. (b) Emission spectra of Hbbpya (50 μM, black line, dimethyl sulfoxide (5% v/v)/PBS), GSH (100 μM), **[1]Cl_2** (50 μM), and of a **[1]Cl_2:GSH** mixture (50:100 μM) 2 min after mixing (green line). (c) ^{1}H NMR spectra of a mixture of **[1]Cl_2:GSH** (3.7 mM:7.4 mM) in D_2O. (d) Hypothesized reaction between **[1]Cl_2** and 2 equiv of GSH.*

DOI: 10.31635/ccschem.023.202303190
Citation: *CCS Chem.* **2024**, 6, 783–797
Link to VoR: https://doi.org/10.31635/ccschem.023.202303190

spectrum, indicating the (meta)stability of the newly formed gold species at this stage. The peaks in the aromatic region remained symmetrical but differed from the peak of the free ligand, suggesting the formation of a new symmetrical gold species. No peaks corresponding to a Au-GSH adduct were seen in the NMR spectrum,[40] indicating that GSH did either not bind to the Au(I) ion in such conditions, or that the binding was dynamic enough not to be observed by ^{1}H NMR.[63] Meanwhile, the precipitate obtained after 24 h was isolated and its ^{1}H NMR spectrum showed it was the **Hbbpya** ligand (Supporting Information Figure S11). We also analyzed solutions of the gold complexes after the reaction with GSH using ESI-MS. As shown in Supporting Information Figure S12, the peaks corresponding to the protonated or oxidized chelator, $[GSH+H]^+$ or $[GSSG+H]^+$, were found. However, we could not detect any other peak corresponding to the association between GSH and a Au(I) center, suggesting that Au(I) ions may exist as isolated—or weakly bound—entities in solution. Overall, we hypothesize that the reaction shown in Figure 2d to occur, in which the Au(III) complex **[1]$^{2+}$** was reduced to Au(I) by GSH to afford GSSG and a transient Au(I) species partially coordinated, in a symmetrical fashion, to **Hbbpya**. This metastable Au(I)-**Hbbpya** species was not stable, and finally released free Au(I) ions and free **Hbbpya** which, at these concentrations, precipitated from water.

Along with GSH, serum proteins represent a major source of thiols with which Au(III) compounds also react. To study the reactivity of **[1]Cl$_2$** with these thiols, we further studied the evolution of the UV–vis spectrum of **[1]Cl$_2$** (50 μM) in cell culture medium (Opti-MEM), either with or without fetal calf serum (FCS, 2.5% v/v). As shown in Supporting Information Figure S13, it was observed that, within 30 min, the absorbance of **[1]Cl$_2$** remained stable in the absence of FCS. However, when FCS was present in the medium, rapid changes of the UV–vis spectrum were observed 2 min after the addition of **[1]Cl$_2$**, while over 24 h all MLCT absorption bands of the complex around 450 nm had disappeared. Unlike in D_2O, no precipitate of the released ligand was found in the Opti-MEM cell-growing medium, which might be attributed to the intrinsic interaction of FCS with hydrophobic organic compounds.[64] To determine whether the released ligand would aggregate as particles after the reaction, dynamic light scattering measurements were conducted. As shown in Supporting Information Figure S14, **[1]Cl$_2$** and **[2]Cl** remained in a nonaggregated, hence molecular form, when dissolved in Opti-MEM solution without FCS. However, upon adding 10% v/v FCS, both compounds formed large micrometer-scale aggregates due to the fast reduction of Au(III) into Au(I) and concomitant release of the polypyridyl ligand. **[3]OAc** exhibited significant microparticle aggregation in Opti-MEM without FCS, probably due to its superior hydrophobicity. These results suggest that, similar to GSH, FCS can react with **[1]Cl$_2$** and **[2]Cl**, most probably via thiol reduction, to generate new Au(I) species and release the free Hbbpya ligand, which remained dissolved, at the concentrations used in this experiment, in Opti-MEM medium.

Table 1 | *Half Maximal Effective Concentrations (EC_{50} in μM) of Gold Complexes **[1]Cl$_2$**, **[2]Cl**, **[3]OAc**, and Cisplatin (Control) Towards 2D Cancer Cell Line Monolayers and 3D Lung (A549) Multicellular Tumor Spheroids, in Normoxic (21% O_2) and Hypoxic (1% O_2) Conditions. 95% Confidence Interval (CI over Three Independent Biological Experiments, in μM) Are Also Indicated*

Complex		EC_{50} (μM) Cell Line A549	±CI	A431	±CI	A375	±CI	MCF-7	±CI	A549-3D	±CI
[1]Cl$_2$	Normoxic	1.1	+0.05 −0.05	1.2	+0.1 −0.1	1.2	+0.08 −0.07	0.47	+0.04 −0.05	1.9	+1 −0.8
	Hypoxic	2.3	+0.4 −0.3	1.1	+0.2 −0.2	1.9	0.3 −0.3	1.7	+0.4 −0.3	—	
[2]Cl	Normoxic	1.4	+0.1 −0.1	2.1	+0.2 −0.1	1.3	+0.09 −0.09	1.8	+0.4 −0.3	2.0	+1 −0.7
	Hypoxic	1.1	+0.2 −0.2	1.8	+0.3 −0.3	1.2	+0.2 −0.2	2.6	+0.3 −0.3	—	
[3]OAc	Normoxic	1.6	+0.1 −0.1	1.7	+0.2 −0.2	0.08	+0.01 −0.01	0.8	+0.4 −0.2	0.38	+0.09 −0.08
	Hypoxic	3.0	+0.8 −0.7	5.0	+3.0 −1.0	0.08	+0.03 −0.02	2.4	+0.6 −0.5	—	
Cisplatin	Normoxic	4.5	+0.7 −0.6	1.8	+0.5 −0.4	1.2	+0.1 −0.1	3.6	+1.2 −0.9	1.6	+0.3 −0.3
	Hypoxic	24	+11 −5	13	+4 −3	3.4	+0.8 −0.7	—		—	

DOI: 10.31635/ccschem.023.202303190
Citation: *CCS Chem.* **2024**, 6, 783–797
Link to VoR: https://doi.org/10.31635/ccschem.023.202303190

Biological properties

The cytotoxicity of the three gold complexes was assessed on four different cancer cell lines: lung cancer A549, skin cancer A431, melanoma cancer A375, and breast cancer MCF-7. Cells were treated with each drug for 72 h under normoxic (21% O_2, 5% CO_2, 37 °C) and hypoxic (1% O_2, 7% CO_2, 37 °C) conditions. The SRB assay was used as an end-point assay to quantify cell viability of the 2D cell monolayers in treated versus untreated wells;[65] cisplatin was used as a control. The half-maximal effective concentrations (EC_{50}) and dose-response curves are reported in Table 1 and Supporting Information Figure S15, respectively.

All the complexes showed low EC_{50} values (~0.08–2.0 μM) in normoxic conditions, indicating broad-spectrum anticancer properties that were even stronger than that of cisplatin (1.2–5.8 μM). Notably, **[3]OAc** showed a highly efficient antiproliferation effect on A375 skin melanoma cells, with an EC_{50} value of 80 nM, which represents 15-fold higher toxicity compared with cisplatin. Hypoxic cancer cells show different microenvironments and gene expression, which usually deactivates many anticancer drugs.[66] For example, the toxicity of cisplatin decreased by a factor of 5 in A549 cells and by a factor of 7 in A431 cells under hypoxic conditions. By contrast, the three gold complexes still showed high cytotoxicity under hypoxia, characterized by an EC_{50} around 0.08–5 μM, which represented only little variations compared with their normoxic EC_{50} values. This result suggested that these gold complexes were able to overcome drug deactivation occurring in hypoxic cancer cells.[67]

Many metallodrugs have been reported that kill cancer cells by inducing apoptosis. Here, we used the Annexin V/PI double-staining assays to detect apoptosis in A549 cancer cells treated with the complexes. As shown in

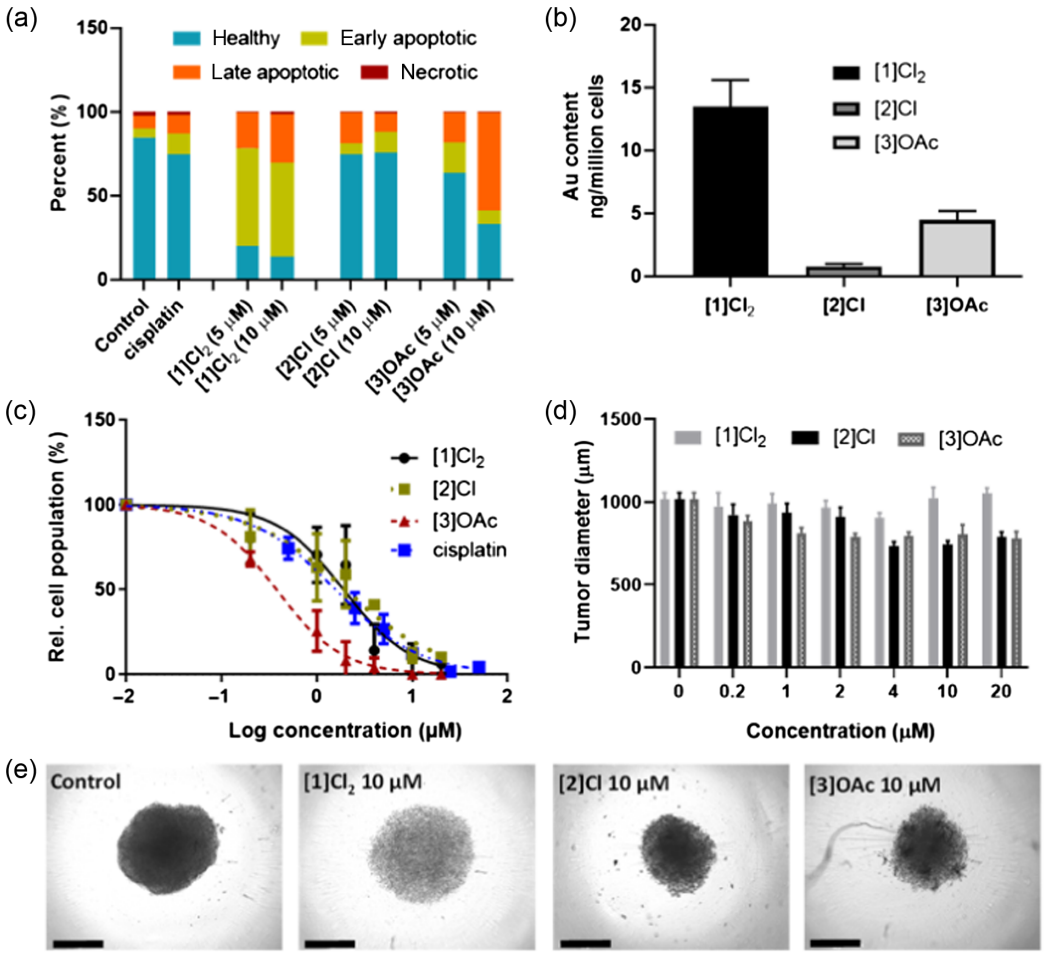

Figure 3 | *(a) Flow cytometry quantification of healthy, early apoptotic, later apoptotic, and necrotic A549 cells after treatment with cisplatin (10 μM),* ***[1]Cl₂*** *(5 μM),* ***[2]Cl*** *(10 μM). or* ***[3]OAc*** *(5 μM) for 24 h. (b) Intracellular Au content (ICP-MS) of A549 cells 24 h after treatment with* ***[1]Cl₂***, ***[2]Cl*** *or* ***[3]OAc*** *(1 μM). (c) Dose–response curves for A549 tumor spheroids incubated with gold complexes and cisplatin. (d) Tumor spheroid diameters after treatment with complexes in different concentrations for 72 h. (e) Brightfield images of multicellular tumor spheroids in control or treatment with gold complexes (scale bar: 500 μm).*

DOI: 10.31635/ccschem.023.202303190
Citation: *CCS Chem.* **2024**, 6, 783–797
Link to VoR: https://doi.org/10.31635/ccschem.023.202303190

Figure 3a and Supporting Information Figure S16, the A549 cell control group showed mostly healthy cells (AV−/PI−, 84.9%), while cells treated with one of the complexes **[1]Cl$_2$**-**[3]OAc** (5 and 10 μM) for 24 h showed a lowered count of healthy cells (5 μM: 20% for **[1]Cl$_2$**, 74.5% for **[2]Cl**, and 63.5% for **[3]OAc**; 10 μM: 13.4% for **[1]Cl$_2$**, 75.5% for **[2]Cl**, and 32.9% for **[3]OAc**), accompanied with an increased count of early (AV+/PI−) and late (AV+/PI+) apoptotic cells. Overall, these results demonstrate that the three gold complexes provoke apoptotic cell death and that **[1]Cl$_2$** is by far the most potent complex of the series.

The drug uptake efficiency is highly relevant to the cytotoxicity of metallodrugs. ICP-MS was hence used to determine the Au content in A549 cells 24 h after treatment with the gold complexes (1 μM). As shown in Figure 3b, **[1]Cl$_2$** was most efficiently taken up (13.5 ng Au/million cells), followed by **[3]OAc** (4.45 ng Au/million cells) and **[2]Cl$_2$** (0.76 ng/million cells), which represented significant variations from one compound to the other. Considering that the EC_{50} values for A549 cells were nearly identical, averaging around 1.5 μM for all three gold complexes, it can be inferred that the cellular uptake efficiency of gold did not significantly impact the cytotoxicity of these compounds towards A549 cells. Instead, cytotoxicity appears to be more influenced by the nature and localization of the tetrapyridyl ligands within the cellular environment. We further evaluated the cytotoxicity of the gold-free ligands in A549 cells and found that they all showed EC_{50} values that were comparable with that of their gold complexes (1.4–2.4 μM, see Supporting Information Figure S17). This surprising result suggested that the toxicity of the gold(III) complexes in the main may be attributed to the ligands released after the complexes had been reduced in the medium. However, the trend that more Au cellular uptake cell groups also showed more apoptotic percentages (**[1]Cl$_2$** > **[3]OAc** > **[2]Cl$_2$**) suggested a positive correlation between Au internalization and apoptosis pathway of A549 cells.

Multicellular tumor spheroids have been proposed as a more suitable model for prescreening anticancer drugs because they provide a valuable mimic of nutrient and drug penetration observed in in vivo tumors.[56,68] The extent of damage to multicellular tumor spheroids can be assessed using various parameters, including cell number, tumor diameter, and contrast. First, we evaluated the cytotoxicity (i.e., relative cell population) of the three gold complexes on A549 tumor spheroids using the Cell Titer Glo 3D adenosine triphosphate (ATP) quantification as end-point assay.[65] As shown in Figure 3c, the three complexes showed significant cytotoxicity in multicellular tumor spheroids, characterized by EC_{50} values around 1 μM, comparable with that of cisplatin. The diameter and contrast of the multicellular tumor spheroids were observed via the bright channel of fluorescence microscopy. The tumor diameters decreased upon dose increase (Figure 3d). However, for **[1]Cl$_2$**, the spheroid diameters were abnormally increased at the concentration of 10 and 20 μM, which could be attributed to the damage and expansion of spheroid cores. Meanwhile, after being treated with gold complexes (10 μM) for 72 h, the tumor contrast was significantly decreased compared with the control group, suggesting the loss of cells in the treated tumor spheroids (Figure 3e). In summary, cytotoxicity evaluation using an SRB assay (2D) or a Cell Titer Glo ATP quantification (3D) demonstrated that the three gold complexes exhibited excellent anticancer abilities in vitro. On the other hand, it should also be noted that the gold complexes were reduced in the cell medium before they reached the cancer cell surface. Thus, their cytotoxicity may mainly be attributed to the released ligands, while the Au(I) species may accelerate apoptotic cell death.

Lysosome imaging, dysfunction, and protein interaction

Numerous cytotoxic gold(III) and gold(I) complexes have been documented for their activity as TrxR inhibitors. Simultaneously, several polypyridyl ligands have been investigated for their role as regulators of potassium channels, either in the cell membrane or within specific organelles like lysosomes and mitochondria.[43–45,69,70] Lysosomal potassium channels are essential for the lysosome physiological function, including lysosomal calcium signaling and autophagy.[69] Numerous reports have demonstrated that the dysregulation of lysosomal potassium channels can impact both the lysosomal membrane potential and pH stability. Such dysregulation can subsequently lead to lysosomal membrane permeabilization (LMP). It is worth noting that LMP can result in the release of the normally sequestered reactive digestive enzymes found within lysosomes into cytoplasm, a process that effectively damages living cancer cells.[71,72]

As described above, upon reduction via GSH **[1]$^{2+}$** releases the fluorescent ligand **Hbbpya** in PBS (Figure 2b). This release is accompanied by a ninefold emission increase in the 400–500 nm region. Thus, confocal microscopy was used to study the evolution of blue fluorescence in A549 cells treated with the gold compounds to see whether ligand release could be visualized. After treatment with **[1]Cl$_2$**, **[2]Cl**, or **[3]OAc** (20 μM) for 3 h, significant blue emission (420–480 nm) was observed in the cells (Figure 4), suggesting efficient uptake of the ligands after the gold complexes had been reduced, either by FCS or intracellular thiol-containing biomolecules. Moreover, the blue emission of the ligands overlapped well with the green emission from the lysosome green tracker (Pearson coefficient P = 0.58, 0.68, 0.79 for **[1]Cl$_2$**, **[2]Cl**, and **[3]OAc**, respectively), indicating that the released ligands accumulated at the lysosome after a short 3 h treatment.

DOI: 10.31635/ccschem.023.202303190
Citation: *CCS Chem.* **2024**, 6, 783–797
Link to VoR: https://doi.org/10.31635/ccschem.023.202303190

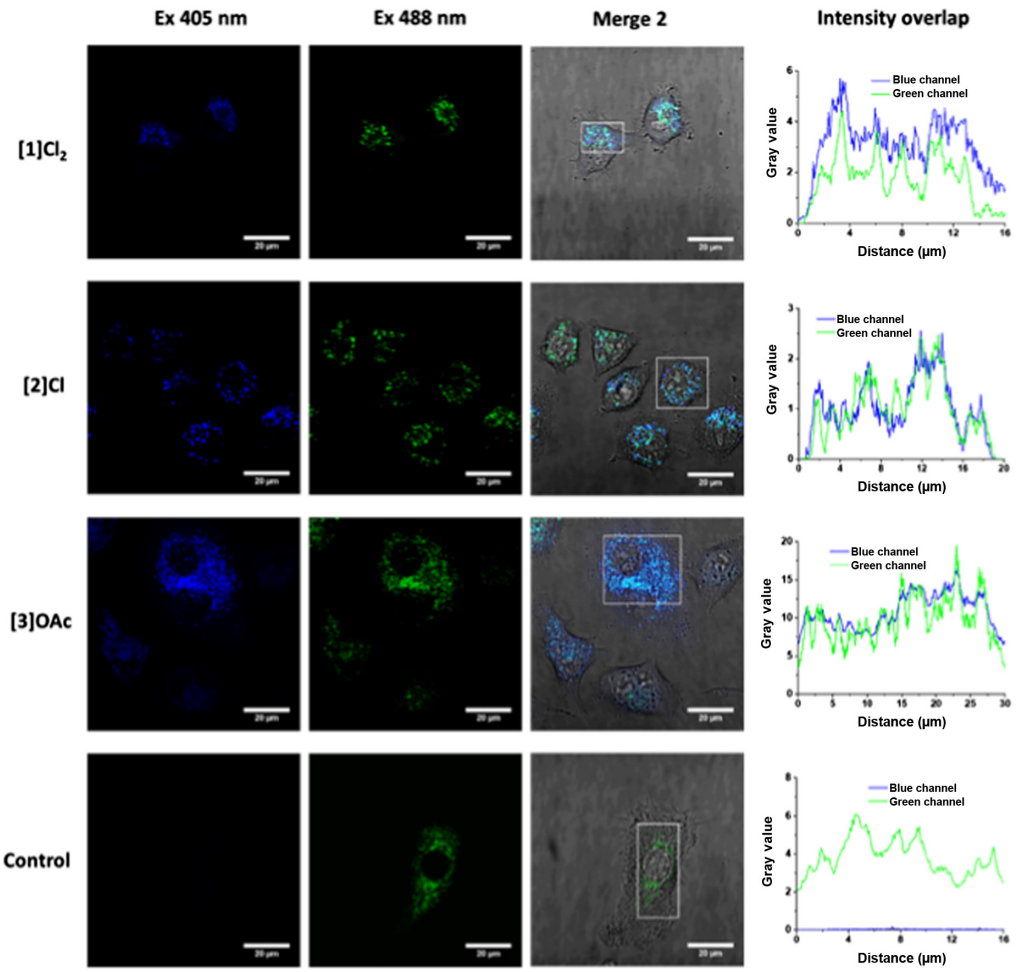

Figure 4 | *Confocal imaging of A549 cells after treatment with* ***[1]Cl$_2$***, ***[2]Cl***, *and* ***[3]OAc*** *(20 μM, Opti-MEM complete medium, 3 h, 405 nm excitation, 410–460 emission) and staining with LTG DND-26 (100 nM, 30 min, 488 nm excitation, 500–560 nm emission). Scale bar: 20 μm.*

To further investigate the effect of gold complexes on lysosomal and cell membrane integrity, A549 cells were costained with the lysosomotropic dye LTG and nucleotide dye PI and studied by flow cytometry. Healthy lysosomes retain more LTG and show higher green staining than damaged lysosomes, while PI only stains the nucleus of cells that have broken cell membranes. As shown in Supporting Information Figure S18 and Table 2, untreated cells (control group) show about 91% (LTG+/PI–) positive lysosomal staining, and just a small population are totally damaged cells (LTG–/PI+), (LG+/PI+), suggesting the healthy situation of lysosome and cells in the negative control group. After being treated with *t*-BuOOH (0.6 mM, a positive control compound that can induce LMP via increased cellular oxidative stress) for 4 h, the percentage of LTG–/PI– and LTG–/PI+ cells increased from 2.69% and 1.93% (negative control) to 24.25% and 34.27%, indicating that many lysosomes broke in such conditions. After treatment with gold complexes, the percentage LTG+/PI– phase was decreased, while the LTG–/PT– phase showed a significant increase with the sequence **[1]Cl$_2$** (8.9%) < **[2]Cl** (12.4%) < **[3]OAc** (24.0%), suggesting that all three gold complexes were able to induce lysosome damage. Our confocal microscopy study of these three compounds on lysosome also showed that the released ligand from **[3]OAC** showed the best lysosome staining, which is in good agreement with the findings of our double-staining flow cytometry analysis.

In light of the reduction of **[1]Cl$_2$-[3]OAc** and the concomitant release of lysosome-targeted polypyridyl ligands, we were motivated to investigate whether the gold complexes could engage in specific interactions with the TrxR enzyme and potassium channels, facilitated by the Au^+ ions and the tetrapyridyl ligands employed in this series. TrxR inhibition experiments were carried out first in cell-free solution by a spectrophotometric assay using commercially available rat liver TrxR. As shown in Table 2, all three gold complexes had submicromolar IC_{50} protein inhibition concentrations (~0.1 μM), indicating that they were very efficient TrxR inhibitors. With such low submicromolar activity, the gold

DOI: 10.31635/ccschem.023.202303190
Citation: *CCS Chem.* **2024**, 6, 783–797
Link to VoR: https://doi.org/10.31635/ccschem.023.202303190

Table 2 | *Lysosome Damage Percent, K_v11.1 Proteins Binding Affinity, and TrxR Enzyme Inhibition of Tetrapyridyl Ligands and Their Gold(III) Complexes*

Compound	Lysosome Damage Percent (%)	TrxR Inhibition IC_{50} (μM)	[^{3}H]dofetilide Binding Remaining (%)[b]	K_v11.1 Binding (%)[c]
Hbbpya	N.D.[a]	N.D.	12 ± 3	88 ± 3
[1]Cl_2	8.94	0.15 ± 0.03	9 ± 1	91 ± 1
H_2bapbpy	N.D.	N.D.	12.6 ± 0.8	87.4 ± 0.8
[2]Cl	12.35	0.10 ± 0.01	6.0 ± 0.4	94.0 ± 0.3
H_2biqbpy	N.D.	N.D.	7.1 ± 0.2	92.9 ± 0.2
[3]OAc	24.06	0.13 ± 0.02	4.2 ± 0.2	95.8 ± 0.2

[a] N.D. = not determined.
[b] Tested concentration = 10 μM.
[c] K_v11.1 binding (%) = 100% − [^{3}H]dofetilide binding remaining (%).

complexes of this report belong to a large group of highly potent gold-based TrxR inhibitors (e.g., auranofin as lead compound of this class showed comparable potency in the same assay, IC_{50} = 0.114 ± 0.012 μM).[36] The strong inhibitory values of the lead compound indicated that TrxR inhibition potentially is an important contributing factor for the cytotoxicity of **[1]Cl_2-[3]OAc**. To confirm this hypothesis in vitro, a second TxR inhibition assay was carried out in living A549 cells for **[1]Cl_2** and **[3]OAc**. Micromolar inhibition concentration values (IC_{50}) were found for **[1]Cl_2** (2.73 ± 0.25 μM) and **[3]OAc** (3.17 ± 1.50 μM), demonstrating that the gold complexes were indeed efficient TrxR inhibitors also after being taken up into the cancer cells. The K_v11.1 potassium channel-binding properties of the tetrapyridyl ligands and their corresponding gold complexes were determined via the radioactive substitution experiment of [^{3}H]dofetilide in HEK293 K_v11.1 cell membranes.[44] Shortly, when a compound binds to the K_v11.1 channel, the binding of reference hERG blocker [^{3}H]dofetilide is decreased, which is used to quantify the K_v11.1 binding efficiency of the tested compounds. As shown in Table 2, at the concentration of 10 μM all the complexes and ligands significantly replaced the remaining [^{3}H]dofetilide and bound to K_v11.1 channel in a range of 88–96%, demonstrating that the potassium channel could be a target both for the ligands and for their gold complexes. One should note that this second assay was performed outside a cellular context; inside a cell, reduction of the gold complex will prevent it from interacting with K_v11.1. However, the lysosome-staining tetrapyridyl ligand release by reduction will block the lysosome potassium channel, which may be the reason why the lysosomal membrane potential tagged by LTG was damaged.

In summary, the concept of gold complexation with polypyridyl ligands emerges as an innovative prodrug design principle. This approach enables the creation of small molecular drugs that can target two distinct proteins: (1) TrxR for the released Au^+ and (2) the the K_v11.1 potassium channel for the polypyridyl ligands. The former is likely to disrupt the redox balance of cancer cells, while the latter probably perturbs the integrity of the lysosomal membrane. Both effects are detrimental to cell survival.

Conclusion

In summary, we have designed and synthesized a series of polypyridyl Au(III) complexes that exhibited thiol-activated Au(III) reduction to Au(I), which is followed by ligand release. All three complexes showed excellent anticancer properties in normoxic 2D cancer cell monolayers and 3D tumor spheroids and remained cytotoxic under hypoxic conditions, suggesting that such compounds are promising alternatives to overcome hypoxia-induced drug deactivation. In particular, the dissociation of the polypyridyl ligand from the gold(I) center led to the restoration of the blue emission of the ligand, which was found to localize within the lysosomes of A549 human lung cells through confocal microscopy. Interestingly, the Au(III) complexes investigated here appear as prodrugs delivering two orthogonal inhibitors: on the one hand, Au^+ ions that target TrxR, and on the other hand a polypyridyl ligand that strongly binds to a potassium channel, thereby destabilizing the lizosome membrane. Both effects combine to produce accelerated apoptosis and a broad-spectrum anticancer property via lysosome damage. In summary, this work extends the established design principle of gold anticancer compounds, which involves TrxR inhibition, to encompass the ligand as a potential bioactive agent that contribute to killing cancer cells.

Supporting Information

Supporting Information is available and includes data on the details of compund synthesis, crystallographic data, cytotoxicity evaluation, cell uptake, and potassium channel binding determination.

DOI: 10.31635/ccschem.023.202303190
Citation: *CCS Chem.* **2024**, 6, 783–797
Link to VoR: https://doi.org/10.31635/ccschem.023.202303190

Conflict of Interest

The authors declare no competing financial interest

Funding Information

X.-Q. Zhou gratefully acknowledges the China Scholarship Council for a personal financial grant (no. 201606200045). This work was also supported by the European Research Council via a Starting Grant, and Dutch Research Council (NWO) for a VICI grant to S. Bonnet.

Acknowledgments

Prof. E. Bouwman is wholeheartedly acknowledged for scientific discussion and support. Dr. S. Zheng is thanked for ICP-MS measurement.

References

1. Kenny, R. G.; Marmion, C. J. Toward Multi-Targeted Platinum and Ruthenium Drugs—A New Paradigm in Cancer Drug Treatment Regimens? *Chem. Rev.* **2019**, *119*, 1058–1137.
2. Qiu, K.; Chen, Y.; Rees, T. W.; Ji, L.; Chao, H. Organelle-Targeting Metal Complexes: From Molecular Design to Bio-Applications. *Coord. Chem. Rev.* **2019**, *378*, 66–86.
3. Imberti, C.; Zhang, P.; Huang, H.; Sadler, P. J. New Designs for Phototherapeutic Transition Metal Complexes. *Angew. Chem. Int. Ed.* **2020**, *59*, 61–73.
4. Zhang, L.; Montesdeoca, N.; Karges, J.; Xiao, H. Immunogenic Cell Death Inducing Metal Complexes for Cancer Therapy. *Angew. Chem. Int. Ed.* **2023**, *62*, e202300662.
5. Xu, Z.; Wang, Z.; Deng, Z.; Zhu, G. Recent Advances in the Synthesis, Stability, and Activation of Platinum(IV) Anticancer Prodrugs. *Coord. Chem. Rev.* **2021**, *442*, 213991.
6. Gul, N. S.; Khan, T.-M.; Liu, Y.-C.; Choudhary, M. I.; Chen, Z.-F.; Liang, H. Pd(II) and Rh(III) Complexes with Isoquinoline Derivatives Induced Mitochondria-Mediated Apoptotic and Autophagic Cell Death in HepG2 Cells. *CCS Chem.* **2021**, *3*, 1626–1641.
7. Qi, F.; Yuan, H.; Chen, Y.; Peng, X.-X.; Wu, Y.; He, W.; Guo, Z. Type I Photoreaction and Photoinduced Ferroptosis by a Ru(II) Complex to Overcome Tumor Hypoxia in Photodynamic Therapy. *CCS Chem.* **2022**, *5*, 1583–1591.
8. Wang, L.; Karges, J.; Wei, F.; Xie, L.; Chen, Z.; Gasser, G.; Ji, L.; Chao, H. A Mitochondria-Localized Iridium(III) Photosensitizer for Two-Photon Photodynamic Immunotherapy Against Melanoma. *Chem. Sci.* **2023**, *14*, 1461–1471.
9. Zhou, X. Q.; Wang, P.; Ramu, V.; Zhang, L.; Jiang, S.; Li, X.; Abyar, S.; Papadopoulou, P.; Shao, Y.; Bretin, L.; Siegler, M. A.; Buda, F.; Kros, A.; Fan, J.; Peng, X.; Sun, W.; Bonnet, S. In Vivo Metallophilic Self-Assembly of a Light-Activated Anticancer Drug. *Nat. Chem.* **2023**, *15*, 980–987.
10. Marmol, I.; Quero, J.; Rodriguez-Yoldi, M. J.; Cerrada, E. Gold as a Possible Alternative to Platinum-Based Chemotherapy for Colon Cancer Treatment. *Cancers* **2019**, *11*, 780.
11. Liu, W.; Gust, R. Update on Metal N-Heterocyclic Carbene Complexes as Potential Anti-Tumor Metallodrugs. *Coord. Chem. Rev.* **2016**, *329*, 191–213.
12. Ott, I. On the Medicinal Chemistry of Gold Complexes as Anticancer Drugs. *Coord. Chem. Rev.* **2009**, *253*, 1670–1681.
13. Smilowicz, D.; Slootweg, J. C.; Metzler-Nolte, N. Bioconjugation of Cyclometalated Gold(III) Lipoic Acid Fragments to Linear and Cyclic Breast Cancer Targeting Peptides. *Mol. Pharm.* **2019**, *16*, 4572–4581.
14. Thomas, S. R.; Bonsignore, R.; Sanchez Escudero, J.; Meier-Menches, S. M.; Brown, C. M.; Wolf, M. O.; Barone, G.; Luk, L. Y. P.; Casini, A. Exploring the Chemoselectivity Towards Cysteine Arylation by Cyclometallated Au(III) Compounds: New Mechanistic Insights. *ChemBioChem* **2020**, *21*, 3071–3076.
15. Lu, Y.; Ma, X.; Chang, X.; Liang, Z.; Lv, L.; Shan, M.; Lu, Q.; Wen, Z.; Gust, R.; Liu, W. Recent Development of Gold(I) and Gold(III) Complexes as Therapeutic Agents for Cancer Diseases. *Chem. Soc. Rev.* **2022**, *51*, 5518–5556.
16. Abas, E.; Belles, A.; Rodriguez-Dieguez, A.; Laguna, M.; Grasa, L. Selective Cytotoxicity of Cyclometalated Gold(III) Complexes on Caco-2 Cells is Mediated by G2/M Cell Cycle Arrest. *Metallomics* **2021**, *13*, 1–16.
17. Srinivasa Reddy, T.; Priver, S. H.; Mirzadeh, N.; Luwor, R. B.; Ganga Reddy, V.; Ramesan, S.; Bhargava, S. K. Antitumor and Antiangiogenic Properties of Gold(III) Complexes Containing Cycloaurated Triphenylphosphine Sulfide Ligands. *Inorg. Chem.* **2020**, *59*, 5662–5673.
18. Zou, T.; Lum, C. T.; Lok, C. N.; Zhang, J. J.; Che, C. M. Chemical Biology of Anticancer Gold(III) and Gold(I) Complexes. *Chem. Soc. Rev.* **2015**, *44*, 8786–801.
19. Jiang, J.; Xiong, X.; Zou, T. Modulating the Chemical Reactivity of Gold Complexes in Living Systems: From Concept to Biomedical Applications. *Acc. Chem. Res.* **2023**, *56*, 1043–1056.
20. Xue, Y.; Li, X.; Li, H.; Zhang, W. Quantifying Thiol-Gold Interactions Towards the Efficient Strength Control. *Nat. Commun.* **2014**, *5*, 4348.
21. Zeng, L.; Kuang, S.; Li, G.; Jin, C.; Ji, L.; Chao, H. A GSH-Activatable Ruthenium(II)-Azo Photosensitizer for Two-Photon Photodynamic Therapy. *Chem. Commun.* **2017**, *53*, 1977–1980.
22. Benhar, M.; Shytaj, I. L.; Stamler, J. S.; Savarino, A. Dual Targeting of the Thioredoxin and Glutathione Systems in Cancer and HIV. *J. Clin. Invest.* **2016**, *126*, 1630–1639.
23. Jia, J. J.; Geng, W. S.; Wang, Z. Q.; Chen, L.; Zeng, X. S. The Role of Thioredoxin System in Cancer: Strategy for Cancer Therapy. *Cancer Chemother. Pharmacol.* **2019**, *84*, 453–470.
24. Gamcsik, M. P.; Kasibhatla, M. S.; Teeter, S. D.; Colvin, O. M. Glutathione Levels in Human Tumors. *Biomarkers* **2012**, *17*, 671–691.
25. Watson, W. H.; Yang, X.; Choi, Y. E.; Jones, D. P.; Kehrer, J. P. Thioredoxin and Its Role in Toxicology. *Toxicol. Sci.* **2004**, *78*, 3–14.
26. Zhang, J.; Li, X.; Han, X.; Liu, R.; Fang, J. Targeting the Thioredoxin System for Cancer Therapy. *Trends Pharmacol. Sci.* **2017**, *38*, 794–808.

DOI: 10.31635/ccschem.023.202303190
Citation: *CCS Chem.* **2024**, 6, 783–797
Link to VoR: https://doi.org/10.31635/ccschem.023.202303190

27. Roder, C.; Thomson, M. J. Auranofin: Repurposing an Old Drug for a Golden New Age. *Drugs R D* **2015**, *15*, 13–20.
28. Ott, I.; Gust, R. Non Platinum Metal Complexes as Anti-Cancer Drugs. *Arch. Pharm.* **2007**, *340*, 117–126.
29. Abhishek, S.; Sivadas, S.; Satish, M.; Deeksha, W.; Rajakumara, E. Dynamic Basis for Auranofin Drug Recognition by Thiol-Reductases of Human Pathogens and Intermediate Coordinated Adduct Formation with Catalytic Cysteine Residues. *ACS Omega* **2019**, *4*, 9593–9602.
30. Marzo, T.; Messori, L. A Role for Metal-Based Drugs in Fighting COVID-19 Infection? The Case of Auranofin. *ACS Med. Chem. Lett.* **2020**, *11*, 1067–1068.
31. Pratesi, A.; Cirri, D.; Fregona, D.; Ferraro, G.; Giorgio, A.; Merlino, A.; Messori, L. Structural Characterization of a Gold/Serum Albumin Complex. *Inorg. Chem.* **2019**, *58*, 10616–10619.
32. Tong, K. C.; Lok, C. N.; Wan, P. K.; Hu, D.; Fung, Y. M. E.; Chang, X. Y.; Huang, S.; Jiang, H.; Che, C. M. An Anticancer Gold(III)-Activated Porphyrin Scaffold That Covalently Modifies Protein Cysteine Thiols. *Proc. Natl. Acad. Sci. U.S. A.* **2020**, *117*, 1321–1329.
33. Fung, S. K.; Zou, T.; Cao, B.; Lee, P. Y.; Fung, Y. M.; Hu, D.; Lok, C. N.; Che, C. M. Cyclometalated Gold(III) Complexes Containing N-Heterocyclic Carbene Ligands Engage Multiple Anti-Cancer Molecular Targets. *Angew. Chem. Int. Ed.* **2017**, *56*, 3892–3896.
34. Zou, T.; Lum, C. T.; Lok, C. N.; To, W. P.; Low, K. H.; Che, C. M. A Binuclear Gold(I) Complex with Mixed Bridging Diphosphine and Bis(N-Heterocyclic Carbene) Ligands Shows Favorable Thiol Reactivity and Inhibits Tumor Growth and Angiogenesis In Vivo. *Angew. Chem. Int. Ed.* **2014**, *53*, 5810–5814.
35. Che, C. M.; Sun, R. W. Therapeutic Applications of Gold Complexes: Lipophilic Gold(III) Cations and Gold(I) Complexes for Anti-Cancer Treatment. *Chem. Commun.* **2011**, *47*, 9554–9560.
36. Schmidt, C.; Albrecht, L.; Balasupramaniam, S.; Misgeld, R.; Karge, B.; Bronstrup, M.; Prokop, A.; Baumann, K.; Reichl, S.; Ott, I. A Gold(I) Biscarbene Complex with Improved Activity as a TrxR Inhibitor and Cytotoxic Drug: Comparative Studies with Different Gold Metallodrugs. *Metallomics* **2019**, *11*, 533–545.
37. Schmidt, C.; Karge, B.; Misgeld, R.; Prokop, A.; Franke, R.; Bronstrup, M.; Ott, I. Gold(I) NHC Complexes: Antiproliferative Activity, Cellular Uptake, Inhibition of Mammalian and Bacterial Thioredoxin Reductases, and Gram-Positive Directed Antibacterial Effects. *Chem. Eur. J.* **2017**, *23*, 1869–1880.
38. Dabiri, Y.; Abu El Maaty, M. A.; Chan, H. Y.; Wolker, J.; Ott, I.; Wolfl, S.; Cheng, X. p53-Dependent Anti-Proliferative and Pro-Apoptotic Effects of a Gold(I) N-Heterocyclic Carbene (NHC) Complex in Colorectal Cancer Cells. *Front. Oncol.* **2019**, *9*, 438.
39. Wenzel, M. N.; Mosca, A. F.; Graziani, V.; Aikman, B.; Thomas, S. R.; de Almeida, A.; Platts, J. A.; Re, N.; Coletti, C.; Marrone, A.; Soveral, G.; Casini, A. Insights into the Mechanisms of Aquaporin-3 Inhibition by Gold(III) Complexes: The Importance of Non-Coordinative Adduct Formation. *Inorg. Chem.* **2019**, *58*, 2140–2148.
40. Zou, T.; Lum, C. T.; Chui, S. S.; Che, C. M. Gold(III) Complexes Containing N-Heterocyclic Carbene Ligands: Thiol "Switch-On" Fluorescent Probes and Anti-Cancer Agents. *Angew. Chem. Int. Ed.* **2013**, *52*, 2930–2933.
41. Zhou, X. Q.; Carbo-Bague, I.; Siegler, M. A.; Hilgendorf, J.; Basu, U.; Ott, I.; Liu, R.; Zhang, L.; Ramu, V.; IJzerman, A. P.; Bonnet, S. Rollover Cyclometalation vs Nitrogen Coordination in Tetrapyridyl Anticancer Gold(III) Complexes: Effect on Protein Interaction and Toxicity. *JACS Au* **2021**, *1*, 380–395.
42. Meanwell, M.; Nodwell, M. B.; Martin, R. E.; Britton, R. A Convenient Late-Stage Fluorination of Pyridylic C-H Bonds with N-Fluorobenzenesulfonimide. *Angew. Chem. Int. Ed.* **2016**, *55*, 13244–13248.
43. Du, L. P.; Tsai, K. C.; Li, M. Y.; You, Q. D.; Xia, L. The Pharmacophore Hypotheses of I(Kr) Potassium Channel Blockers: Novel Class III Antiarrhythmic Agents. *Bioorg. Med. Chem. Lett.* **2004**, *14*, 4771–4777.
44. Carvalho, J. F.; Louvel, J.; Doornbos, M. L.; Klaasse, E.; Yu, Z.; Brussee, J.; IJzerman, A. P. Strategies to Reduce HERG K+ Channel Blockade. Exploring Heteroaromaticity and Rigidity in Novel Pyridine Analogues of Dofetilide. *J. Med. Chem.* **2013**, *56*, 2828–2840.
45. Yu, Z.; van Veldhoven, J. P.; Louvel, J.; t Hart, I. M.; Rook, M. B.; van der Heyden, M. A.; Heitman, L. H.; IJzerman, A. P. Structure-Affinity Relationships (SARs) and Structure-Kinetics Relationships (SKRs) of K_v11.1 Blockers. *J. Med. Chem.* **2015**, *58*, 5916–5929.
46. Felipe, A.; Vicente, R.; Villalonga, N.; Roura-Ferrer, M.; Martinez-Marmol, R.; Sole, L.; Ferreres, J. C.; Condom, E. Potassium Channels: New Targets in Cancer Therapy. *Cancer Detect Prev.* **2006**, *30*, 375–385.
47. Pardo, L. A.; Stuhmer, W. The Roles of K(+) Channels in Cancer. *Nat. Rev. Cancer* **2014**, *14*, 39–48.
48. Zhou, X. Q.; Xiao, M.; Ramu, V.; Hilgendorf, J.; Li, X.; Papadopoulou, P.; Siegler, M. A.; Kros, A.; Sun, W.; Bonnet, S. The Self-Assembly of a Cyclometalated Palladium Photosensitizer into Protein-Stabilized Nanorods Triggers Drug Uptake In Vitro and In Vivo. *J. Am. Chem. Soc.* **2020**, *142*, 10383–10399.
49. Sheldrick, G. M. SHELXT–Integrated Space-Group and Crystal-Structure Determination. *Acta Crystallogr. A: Found. Adv.* **2015**, *71*, 3–8.
50. Yu, Z.; van Veldhoven, J. P. D.; t Hart, I. M. E.; Kopf, A. H.; Heitman, L. H.; Ijzerman, A. P. Synthesis and Biological Evaluation of Negative Allosteric Modulators of the K_v11.1(hERG) Channel. *Eur. J. Med. Chem.* **2015**, *106*, 50–59.
51. Zheng, S.; Reintjens, N. R.; Siegler, M. A.; Roubeau, O.; Bouwman, E.; Rudavskyi, A.; Havenith, R. W.; Bonnet, S. Stabilization of the Low-Spin State in a Mononuclear Iron(II) Complex and High-Temperature Cooperative Spin Crossover Mediated by Hydrogen Bonding. *Chem. Eur. J.* **2016**, *22*, 331–339.
52. van Rixel, V. H. S.; Siewert, B.; Hopkins, S. L.; Askes, S. H. C.; Busemann, A.; Siegler, M. A.; Bonnet, S. Green Light-Induced Apoptosis in Cancer Cells by a Tetrapyridyl

DOI: 10.31635/ccschem.023.202303190
Citation: *CCS Chem.* **2024**, 6, 783–797
Link to VoR: https://doi.org/10.31635/ccschem.023.202303190

Ruthenium Prodrug Offering Two Trans Coordination Sites. *Chem. Sci.* **2016**, *7*, 4922–4929.
53. Simonov, Y.; Bologa, O.; Bourosh, P.; Gerbeleu, N.; Lipkowski, J.; Gdaniec, M. Synthesis and Structural Characterization of Gold(III) Dioximates with Anions $[AuCl_4]^-$ and $[AuCl_2]^-$. *Inorg. Chim. Acta* **2006**, *359*, 721–725.
54. van Rixel, V. H. S.; Busemann, A.; Wissingh, M. F.; Hopkins, S. L.; Siewert, B.; van de Griend, C.; Siegler, M. A.; Marzo, T.; Papi, F.; Ferraroni, M.; Gratteri, P.; Bazzicalupi, C.; Messori, L.; Bonnet, S. Induction of a Four-Way Junction Structure in the DNA Palindromic Hexanucleotide 5′-d (CGTACG)-3′ by a Mononuclear Platinum Complex. *Angew. Chem. Int. Ed.* **2019**, *58*, 9378–9382.
55. Wan, Q.; Yang, J.; To, W. P.; Che, C. M. Strong Metal-Metal Pauli Repulsion Leads to Repulsive Metallophilicity in Closed-Shell d(8) and d(10) Organometallic Complexes. *Proc. Natl. Acad. Sci. U.S.A.* **2021**, *118*, e2019265118.
56. Di Modugno, F.; Colosi, C.; Trono, P.; Antonacci, G.; Ruocco, G.; Nisticò, P. 3D Models in the New Era of Immune Oncology: Focus on T Cells, CAF and ECM. *J. Exp. Clin. Cancer Res.* **2019**, *38*, 117.
57. Poturcu, K.; Demiralay, E. Ç. Determination of pKa Values for Some Benzimidazole and Imidazole Group Drugs Using the Reversed-Phase Liquid Chromatography Method. *J. Chem. Eng. Data* **2020**, *65*, 5617–5626.
58. Martinez, C. H.; Dardonville, C. Rapid Determination of Ionization Constants (p*K*a) by UV Spectroscopy Using 96-Well Microtiter Plates. *ACS Med. Chem. Lett.* **2013**, *4*, 142–145.
59. Carboni, S.; Zucca, A.; Stoccoro, S.; Maiore, L.; Arca, M.; Ortu, F.; Artner, C.; Keppler, B. K.; Meier-Menches, S. M.; Casini, A.; Cinellu, M. A. New Variations on the Theme of Gold(III) C(wedge)N(wedge)N Cyclometalated Complexes as Anticancer Agents: Synthesis and Biological Characterization. *Inorg. Chem.* **2018**, *57*, 14852–14865.
60. Vogler, A.; Kunkely, H. Ligand-to-Ligand and Intraligand Charge Transfer and Their Relation to Charge Transfer Interactions in Organic Zwitterions. *Coord. Chem. Rev.* **2007**, *251*, 577–583.
61. Nakayama, T.; Isobe, T.; Nakamiya, K.; Edmonds, J. S.; Shibata, Y.; Morita, M. Complexes of Diphenylarsinic Acid and Phenylarsonic Acid with Thiols: A ^{1}H and ^{13}C NMR Study. *Magn. Reson. Chem.* **2005**, *43*, 543–550.
62. Giannini, F.; Suss-Fink, G.; Furrer, J. Efficient Oxidation of Cysteine and Glutathione Catalyzed by a Dinuclear Areneruthenium Trithiolato Anticancer Complex. *Inorg. Chem.* **2011**, *50*, 10552–10554.
63. Köster, S. D.; Alborzinia, H.; Can, S.; Kitanovic, I.; Wölfl, S.; Rubbiani, R.; Ott, I.; Riesterer, P.; Prokop, A.; Merz, K.; Metzler-Nolte, N. A Spontaneous Gold(I)-Azide Alkyne Cycloaddition Reaction Yields Gold-Peptide Bioconjugates Which Overcome Cisplatin Resistance in a p53-Mutant Cancer Cell Line. *Chem. Sci.* **2012**, *3*, 2062–2072.
64. Sreedhanya, S.; Jeena, V. R.; Ammu, S.; Aravindakumar, C. T.; Aravind, U. K. Spectroscopic and Theoretical Methods to Probe Protein–Ligand Binding. *Mater. Today Proc.* **2020**, *33*, 1361–1366.
65. van Rixel, V. H. S.; Ramu, V.; Auyeung, A. B.; Beztsinna, N.; Leger, D. Y.; Lameijer, L. N.; Hilt, S. T.; Le Devedec, S. E.; Yildiz, T.; Betancourt, T.; Gildner, M. B.; Hudnall, T. W.; Sol, V.; Liagre, B.; Kornienko, A.; Bonnet, S. Photo-Uncaging of a Microtubule-Targeted Rigidin Analogue in Hypoxic Cancer Cells and in a Xenograft Mouse Model. *J. Am. Chem. Soc.* **2019**, *141*, 18444–18454.
66. Mondal, A.; Paira, P. Hypoxia Efficient and Glutathione-Resistant Cytoselective Ruthenium(II)-p-Cymene-Arylimidazophenanthroline Complexes: Biomolecular Interaction and Live Cell Imaging. *Dalton Trans.* **2020**, *49*, 12865–12878.
67. Denny, W. A. The Role of Hypoxia-Activated Prodrugs in Cancer Therapy. *Lancet Oncol.* **2000**, *1*, 25–29.
68. Nunes, A. S.; Barros, A. S.; Costa, E. C.; Moreira, A. F.; Correia, I. J. 3D Tumor Spheroids as in Vitro Models to Mimic in Vivo Human Solid Tumors Resistance to Therapeutic Drugs. *Biotechnol. Bioeng.* **2019**, *116*, 206–226.
69. Feng, X.; Zhao, Z.; Li, Q.; Tan, Z. Lysosomal Potassium Channels: Potential Roles in Lysosomal Function and Neurodegenerative Diseases. *CNS Neurol. Disord. Drug Targets* **2018**, *17*, 261–266.
70. Cang, C.; Aranda, K.; Seo, Y. J.; Gasnier, B.; Ren, D. TMEM175 Is an Organelle K^+ Channel Regulating Lysosomal Function. *Cell* **2015**, *162*, 1101–1112.
71. Sun, X.; Xu, M.; Cao, Q.; Huang, P.; Zhu, X.; Dong, X. P. A Lysosomal K^+ Channel Regulates Large Particle Phagocytosis by Facilitating Lysosome Ca^{2+} Release. *Sci. Rep.* **2020**, *10*, 1038.
72. Amaravadi, R. K.; Kimmelman, A. C.; Debnath, J. Targeting Autophagy in Cancer: Recent Advances and Future Directions. *Cancer Discov.* **2019**, *9*, 1167–1181.

DOI: 10.31635/ccschem.023.202303190
Citation: *CCS Chem.* **2024**, 6, 783–797
Link to VoR: https://doi.org/10.31635/ccschem.023.202303190